

# Enhancement of human color vision by breaking the binocular redundancy

Bradley S. Gundlach<sup>1</sup>, Alireza Shahsafi<sup>1</sup>, Gregory Vershbow<sup>2</sup>, Chenghao Wan<sup>1,3</sup>, Jad Salman<sup>1</sup>, Bas Rokers<sup>4,5</sup>, Laurent Lessard<sup>1</sup>, Mikhail A. Kats<sup>1,3,5\*</sup>

<sup>1</sup>Department of Electrical and Computer Engineering, University of Wisconsin-Madison

<sup>2</sup>Department of Art, University of Wisconsin-Madison

<sup>3</sup>Department of Materials Science and Engineering, University of Wisconsin-Madison

<sup>4</sup>Department of Psychology, University of Wisconsin-Madison

<sup>5</sup>McPherson Eye Research Institute, University of Wisconsin-Madison

\*Corresponding Author: Mikhail A. Kats

Address: 1415 Engineering Dr, Madison, WI 53706

Email: mkats@wisc.edu

Phone: (608)890-3984

## ABSTRACT

To see color, the human visual system combines the responses of three types of cone cells in the retina – a process that discards a significant amount of spectral information. We present an approach that can enhance human color vision by breaking the inherent redundancy in binocular vision, providing different spectral content to each eye. Using a psychophysical color model and thin-film optimization, we designed a wearable passive multispectral device that uses two distinct transmission filters, one for each eye, to enhance the user’s ability to perceive spectral information. We fabricated and tested a design that “splits” the response of the short-wavelength cone of individuals with typical trichromatic vision, effectively simulating the presence of four distinct cone types between the two eyes (“tetrachromacy”). Users of this device were able to differentiate metamers (distinct spectra that resolve to the same perceived color in typical observers) without apparent adverse effects to vision. The increase in the number of effective cones from the typical three reduces the number of possible metamers that can be encountered, enhancing the ability to discriminate objects based on their emission, reflection, or transmission spectra. This technique represents a significant enhancement of the spectral perception of typical humans, and may have applications ranging from camouflage detection and anti-counterfeiting to art and data visualization.

In humans, the visual system relies on three types of photoreceptor cone cells with different frequency-dependent sensitivities that, when combined, cover the range of wavelengths between 390 and 700 nm (Fig. 1a) (1). In typical, healthy humans, the three cone types (labeled “S” for short wavelengths, “M” for medium, and “L” for long) are sensitive to approximately 390 - 530 nm, 400 - 670 nm, and 400 - 700 nm, and very roughly correspond to blue, green, and red colors, respectively (2). The three cone types utilize different versions of a photoreceptor protein (photopigment), resulting in the distinct frequency sensitivity of each cone type (3). Incident photons excite the photopigment, which allows the cone cells to detect the photon flux with respect to a given photopigment spectral sensitivity. This response is then relayed through retinal ganglion cells, to the optic nerve, and then the brain, where it is processed further by the neuronal color-coding system to produce a color sensation (4).

Though this process provides a significant amount of spectral information to the observer, it also introduces a degree of ambiguity, due to the compression of the spectrum of each region within the visual field into three color channels (corresponding to the three cone types). Because of this compression, there exist many spectra that result in similar cone responses, and subsequently appear as the same color. This phenomenon, known as metamerism, is a limitation of human color vision (5, 6). The number of cone types governs the degree to which metamerism is present, such that a hypothetical increase in the number of distinct cone types would result in a decrease in the overall number of possible metamers. For example, some animals, such as the Eurasian blue tit (*Cyanistes caeruleus*), evolved to have four cone types (Fig. 1c) (7). Conversely, decreasing the number of cone types increases the overall number of possible metamers, and reduces the amount of spectral information provided by the visual system. For example, some humans with color-vision deficiencies lack one or more of the three typical cone types, and are thus unable to distinguish certain colors depending on the type of deficiency (8–10).

Several studies have reported that some humans express an additional mutated L cone, resulting in a total of four cone types (tetrachromacy) (11–13). While significant debate remains, reports suggest that some of those individuals can take advantage of the information provided by the fourth photopigment and “perceive significantly more chromatic appearances” compared to typical, healthy humans with three cone types (trichromats) (14–16). More broadly, it is reasonable to infer that an additional cone type enhances spectral perception, provided subsequent neural processing can capitalize on its presence.

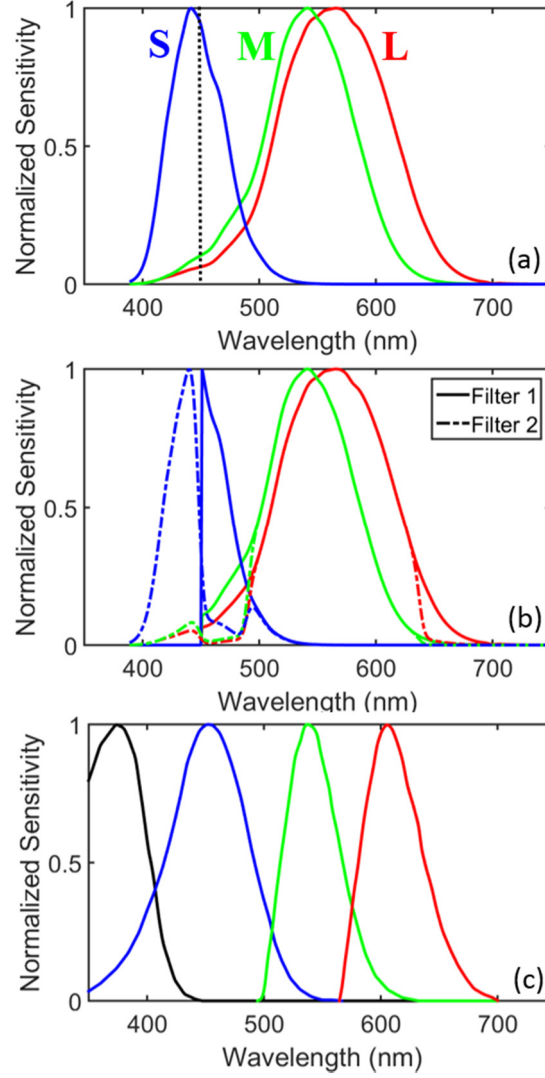


**Figure 1:** (a) Normalized spectral sensitivities of cone types for a typical human (1). (b) Sensitivities of the four *effective* cone types created using the two filters described in this work. (c) Normalized spectral sensitivities of cone types for a Eurasian blue tit (*Cyanistes caeruleus*) (7).

In this work, we demonstrate a method to simulate tetrachromatic (and higher dimensional) color vision in typical trichromatic humans by increasing the *effective* number of cone types in the visual system. Our approach works by breaking the binocular redundancy of the two eyes, providing different spectral content to each eye via a wearable passive multispectral device comprising two optical transmission filters (Fig. 2). Each filter selectively attenuates different wavelength bands to yield effective cone sensitivities (*i.e.*, the products of the cone sensitivities and the filter transmission spectra) that are different between the two eyes. We used a standard psychophysical model that predicts the perceived color of a given spectrum to optimize the optical filters comprising the passive multispectral device. These filters are designed to

enhance the ability of a typical trichromatic viewer to discriminate metameric spectra while limiting adverse effects such as color clashing and the introduction of additional metamers. We experimentally demonstrated one particular filter design that splits the response of the short-wavelength (S) cone, thus transforming the trichromatic visual system into one that emulates tetrachromatic (four-cone) vision. This design allows users to differentiate between various blue, purple and violet metamers, without apparent adverse effects. We posit that the extra spectral information can be understood as creating a set of new “meta-colors”, distinguishable from colors perceived without the filters. The methods introduced here can, in principle, be used to split any cone or combination of cones, resulting in a visual system with up to six effective cone types.

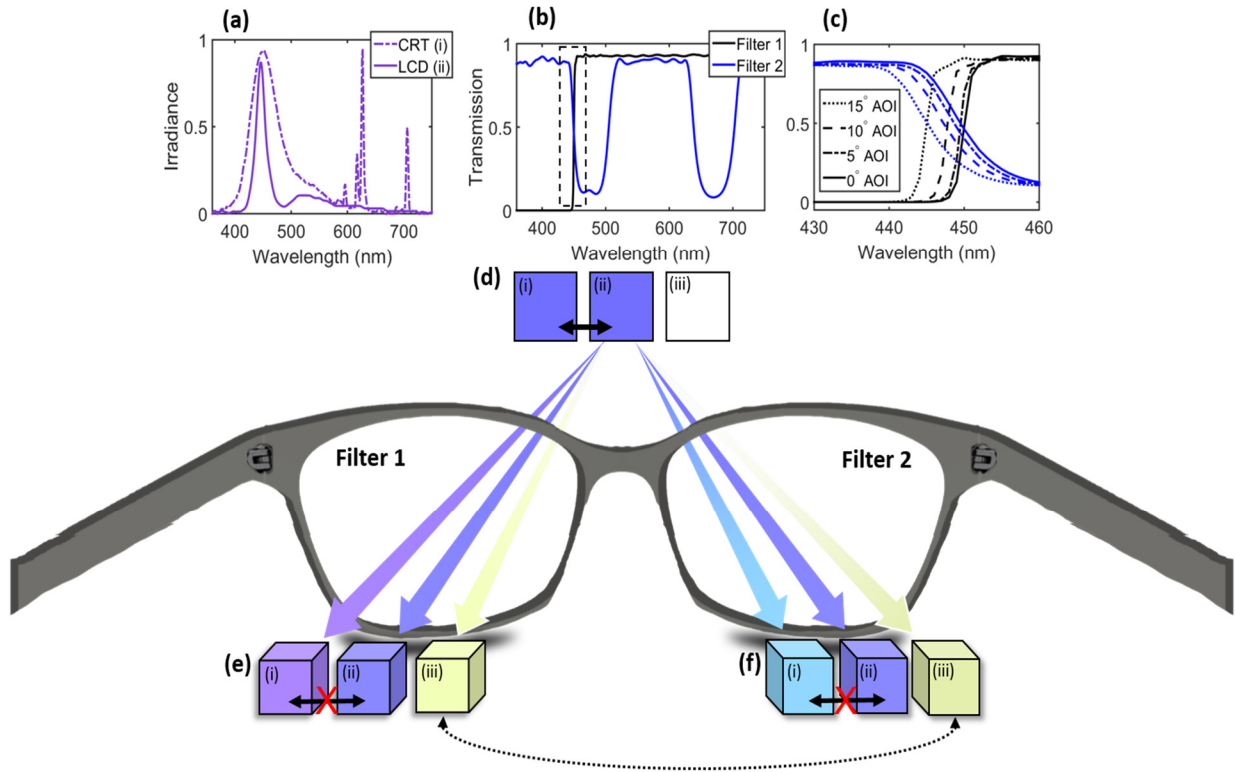


**Figure 2:** Schematic of our filter-based cone partitioning method, consisting of two distinct transmission filters. Plot (a) shows the spectra of a sample pair of metamers, (i) and (ii), which appear as the same purple color and were experimentally generated using two different displays (CRT and LCD). The measured transmission spectra of filters 1 and 2 are given in (b); (c) shows a magnified view of one of the transition regions of the filters, demonstrating their angular response. The color samples in (d) represent the perceived colors of spectra (i-iii), where spectrum (iii) is CIE D65 white light, in the absence of any filters. The samples in d(i) and d(ii) are the same color (*i.e.*, they are metamers), and d(iii) is pure white. (e) and (f) show the colors corresponding to spectra (i-iii) as observed through filters 1 and 2; spectra (i) and (ii) no longer map to the same color. Samples e(iii) and f(iii) are approximately the same perceived color, which is a consequence of the white-balance design constraint that is enforced to limit color clashing.

Previously, there have been attempts to enhance vision in color-deficient individuals using a single optical filter in front of both eyes that serves to block bands of “confusing” wavelengths, for example to help individuals with red-green color-vision deficiency to differentiate red and green objects (17). The use of a single filter in this manner helps to distinguish a certain subset of existing metamers (for both typical and color-deficient individuals), but also creates a new set of metamers equal in dimensionality. Conversely, our use of two distinct filters (one per eye) decreases the overall number of potential metamers, even for typical individuals with trichromatic vision. Each distinct filter placed in front of the eye results in a separate set of metamers, thereby allowing the user to distinguish metamers so long as at least one of the filters “splits” the metameric pair. The reduction in the overall number of metamers is a consequence of each filter creating a distinct set of metameric spectra, thus decreasing the overall effect of metamerism. We note that a related approach of using two simple band-pass filters, one for each eye, was previously demonstrated to increase the dimensionality of color vision in dichromatic individuals (those with two functioning cone types) (18). Other studies have used a single filter in front of one eye of a color deficient individual, leaving the other eye unaffected, and have observed increases in color-space dimensionality (though adverse stereoscopic effects were observed) (19–21). Unlike these works, our goal is to enhance the dimensionality of a trichromatic user’s visual system to beyond that of a typical human while minimizing any adverse effects. To our knowledge, no study has investigated such an approach for the enhancement of healthy human vision, or provided a rigorous design method for such an application.

Figure 1(a) shows that the responsivity of the S cone has little overlap with those of the M and L cones, making it possible to change the effective response of the S cone using optical filters without significantly affecting the other cone types. We take advantage of this lack of overlap to simplify the design, and demonstrate a proof-of-concept pair of filters that splits the response of the S cone between the two eyes. To provide parity between eyes, we partitioned the S cone responsivity such that each eye retains approximately half of the original response spectrum (Fig. 1(b)). We also enforced a “white-balance” design constraint, ensuring that the transmission of broadband white light through both filters results in a similar color in both eyes. This condition ensures that the filters function properly in their intended environment (daylight in this work), without resulting in clashing between the two eyes (22). Here, we define white light according to the International Commission on Illumination (CIE) Illuminant D65 standard, which represents natural daylight (23). To quantify color differences, the CIE76  $\Delta E$  standard is used (24, 25):

$$\Delta E_{ab} = \sqrt{(L_2 - L_1)^2 + (a_2 - a_1)^2 + (b_2 - b_1)^2} \quad (1),$$

where  $(L_1, a_1, b_1), (L_2, a_2, b_2)$  are tristimulus values in the CIELAB color space, and are calculated directly from the spectra (See supplementary for more information) (26). Tristimulus values are a set of three numbers that represent a color in a particular color space. While the red-green-blue (RGB) color space is

the most recognized, the CIELAB space is designed to be “perceptually uniform”, making it easy to quantify color differences (Eqn. 1).

Initially, a basic optimization routine implementing longpass and bandstop filters was used to understand the effect that splitting the S cone has on color balance. This filter configuration was chosen for convenience, as it is the simplest way to split the S cone while minimizing the effect on the M and L cones. From this naïve solution, an optimal cut-on and cut-off wavelength for the two filters was found to be 450 nanometers, which matches intuition as the S-cone sensitivity peaks at this wavelength (see Supplementary). This naïve solution is not optimal because the S cone response overlaps somewhat with the M and L cone responses (Fig. 1(a)), so neatly splitting the S cone response into two sections results in one filter attenuating the tails of the M and L cones, affecting the color balance. To fully split the S cone while maintaining color balance, a second stop-band region was introduced at longer wavelengths (Fig. 1(c), Fig. 2(b, c)). With this configuration, filter 1 attenuates the short-wavelength tails of the M and L cones, while filter 2 attenuates the long-wavelength tails of the M and L cones, yielding good white-balance.

For convenience, and to save on manufacturing costs, a commercially available 450 nm longpass filter (450LP Rapidedge, Omega Optical) was chosen as filter 1. We then optimized filter 2, adjusting the position and amplitude of the stop bands such that the  $\Delta E$  color difference for D65 white light between filters 1 and 2 was minimized. The optimization was performed using the constrained optimization by linear approximation (COBYLA) minimization routine, implemented in the Python SciPy package (27, 28). The transmittance was constrained between 5 and 15% in the stop bands, and between 80 and 95% in the pass bands, to allow for high throughput as well as ease in manufacturing (*i.e.*, very high or low broadband transmission is difficult to attain). This procedure yielded an optimized response for filter 2 with stopbands at 450 - 500 nm and 630 - 680 nm and stopband/passband transmittance of 10% and 90%, respectively (Fig. 2(b,c)). During this procedure, we were not particularly concerned with finding a global optimum; instead, a reasonably optimal solution is sufficient. The optimization process is described in more detail in the Supplementary.

We implemented the transmission function of filter 2 using a thin-film dielectric stack of alternating layers of silicon oxide ( $\text{SiO}_2$ ) and tantalum oxide ( $\text{Ta}_2\text{O}_5$ ), common transparent materials with refractive indices of 1.46 and 2.15, respectively. The thicknesses and arrangement of layers were optimized using commercial software (Optilayer), obtaining a thin-film stack that reasonably matches the desired transmission spectrum (see Supplementary for details). The thin-film layers were deposited on NBK-7 optical glass using sputtering (Iridian Spectral Technologies). Figure 2(b,c) shows the measured transmission spectra of filters 1 and 2 at normal and oblique incidence.

To test the performance of our design, we constructed a setup that generates pairs of metamers (Fig. 3(a,b)). Two displays with very different emission spectra — a True HD-IPS liquid crystal display (LCD) on a LG G3 smartphone and a conventional cathode ray tube (CRT) monitor (Dell E770P) — were used to display a large block of the same color (See supplementary for a detailed comparison of the display types). The displays rely on different emission mechanisms, and thus use different spectra to generate the same perceived color (i.e. generating a metamer pair) (29, 30). A large 50/50 beam splitter (Edmund Optics) was used to present the two images next to each other such that a side-by-side comparison could be made (Fig. 3(a,b)). Without the use of either filter, the two images appeared to be nearly the same color (Fig. 3c). However, when observed through either of the filters, the two images could be easily differentiated. Note the image in Fig. 3(b) is a photograph, but the color samples in Fig. 3c are not; instead, they are rendered from spectra acquired using a free-space spectrometer (Ocean Optics FLAME VIS-NIR with cosine corrector). The filters were applied digitally to prevent the introduction of errors due to the differences between the spectral response of the camera pixels and the response of human cones (see supplementary). Subjectively, we observed that, by looking at a particular color through both filters simultaneously (e.g. filter 1 over the left eye, filter 2 over the right), a “meta-color” is observed, which appears to be different from the original perceived color and both individual filtered perceived colors. This meta-color is a manifestation of the “extra” effective cone type created by the pair of filters, and demonstrates the increased information relayed to the visual system resulting from the partitioning of the S cone.

To demonstrate the utility of our wearable passive multispectral device in a more natural setting, we acquired a hyperspectral image of a complex scene, and applied the filters digitally (Fig. 4). The scene included a variety of blue and violet objects, including blocks of color made using paints and pastels, plants, and a Morpho butterfly featuring a structural blue color (31). The image was obtained using a Middleton Spectral Vision MSV-500 High Sensitivity VNIR hyperspectral camera.

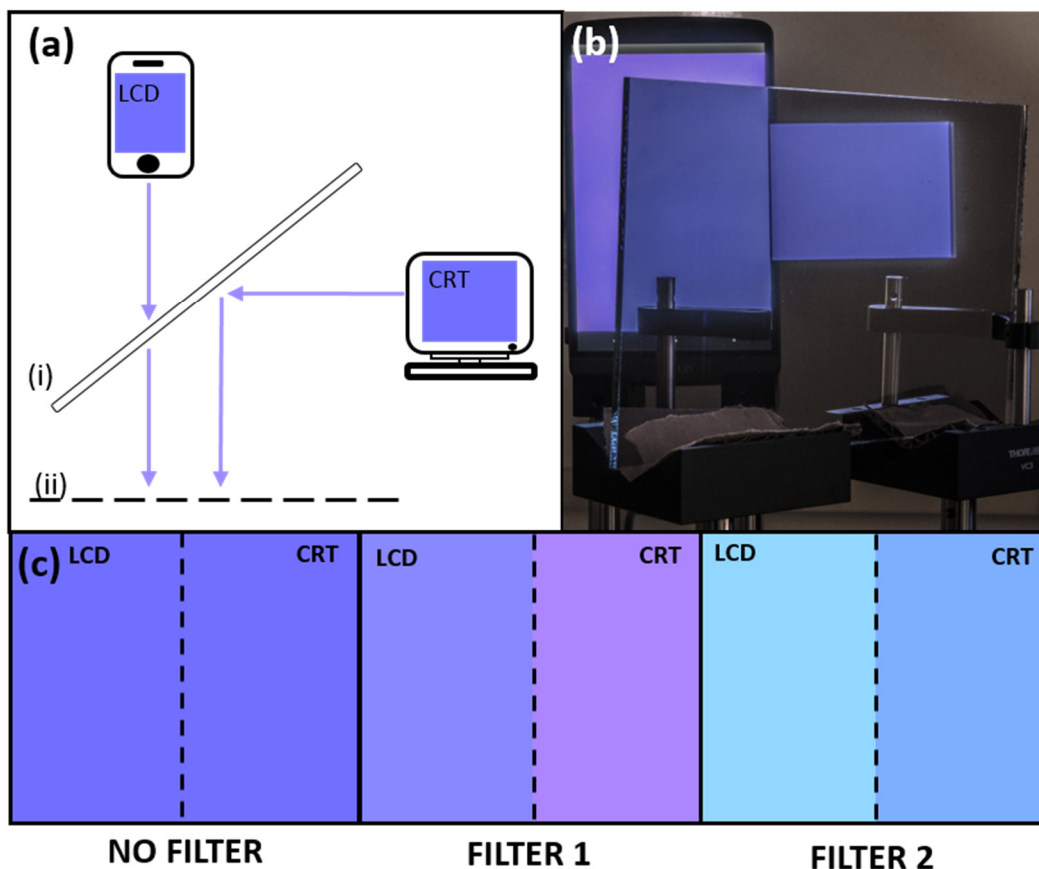


**Figure 3:** (a) Schematic of the metamer generation setup; (i) is a 50/50 beam splitter, and (ii) is the viewing plane. (b) Photograph taken at position (ii) in the schematic. (c) Purple metameric blocks of color generated by the monitors through no filter, filter 1, and filter 2, respectively, showing that the metamers can be distinguished using either filter 1 or filter 2

The enlarged images in Fig. 4(d) show the butterfly wing next to six similarly colored samples made using oil pastels, with no filters applied. In Fig. 4(e) and Fig. 4(f), filters 2 and 1, respectively, are applied to these enlarged images. The numbers in each panel represent the CIE  $\Delta E$  color difference between the oil pastel color and the butterfly wing, averaged over a small area to reduce pixel noise. Using filter 2 (Fig. 4(f)), the appearance of the butterfly wing becomes more dissimilar to the pastel samples compared to no filter (*i.e.*, the butterfly “blue” becomes easier to distinguish from the pastel “blue” using the filter). This again demonstrates the effect of partitioning the S cone to provide more spectral information. The improvement is absent for filter 1 (Fig. 4(e)), demonstrating the need for both filters in the design. We note that each filter creates a new set of metamers that may have been distinguishable before; by using two filters, the set of overlapping newly created metamers becomes significantly smaller. Therefore, as long as at least one filter creates an increase in contrast, more spectral information is



communicated to the visual system while decreasing the overall number of possible metamers. We note that, although a slight yellow/green tint is applied to both filtered images, Fig. 4(b) and Fig. 4(c) have similar “white-balance” due to the white-balance condition enforced during the design process.

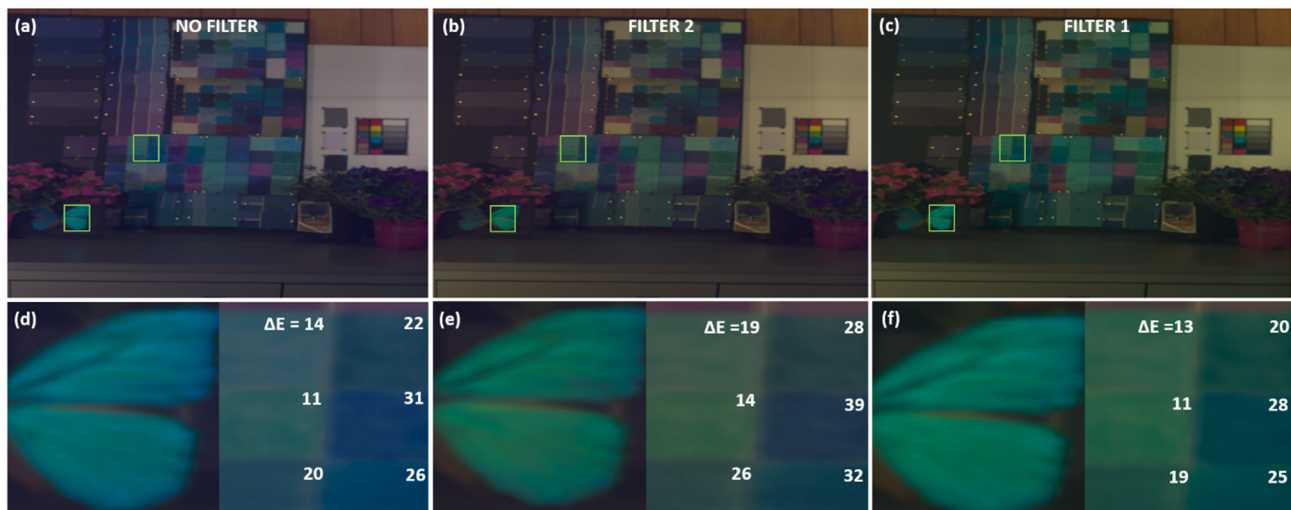


**Figure 4:** (a) RGB rendering of a hyperspectral image with natural and artificially colored objects, with no filter applied. (b) The render with filter 2 applied, and (c) the render with filter 1 applied. (d) Magnified view of butterfly wing and paint samples (outlined in green in (a)). (e) and (f) are the same samples as in (d), with filters 2 and 1 applied, respectively. The numbers inside each paint sample are the  $\Delta E$  color difference, rounded to the nearest integer, between the paint sample and the butterfly wing with each respective filter applied.

Broadly stated, the number of cone types and their frequency dependent responsivities determines the extent to which metamerism is a limitation to the visual system. Our method increases the effective number of cone types of a viewer, which decreases the number of potential metamers. In general, quantitatively determining this decrease in metamer frequency is difficult because the set of possible metamers is not bounded. Nevertheless, by one metric, we estimate a decrease in metamer frequency by one-to-two orders of magnitude when using our passive multispectral device (see supplementary information). By the same metric, a single-filter system such as the one described in ref. [17] provides no decrease in the frequency of apparent metamers. A single-filter system simply shifts metamers to a different part of the color space, while our two-filter approach yields a significant reduction of the frequency of apparent metamers.

By breaking the inherent chromatic redundancy in binocular vision, our method provides the user with more spectral information than he/she would otherwise receive. In the present design, the S cone is split using a pair of filters that results in vision capability consistent with a visual system that utilizes four cone types (tetrachromacy). Although the current demonstration splits the S cone, which is more sensitive to blue-colored objects that are not very common in nature, it is possible to use similar methods to design filters that more-strongly affect green and red metamers that are more common (32). While the potential for natural tetrachromacy in a fraction of the population has received both academic and popular interest recently (14–16), the technology demonstrated here has the potential to provide tetrachromatic vision to anyone with typical, healthy trichromatic vision. The extent to which observers can (or can learn) to take advantage of the additional spectral information will be probed in future work.

Given two eyes and three types of cones, it should be possible to increase the number of effective cones up to six using our approach, and potentially even more with spatial or temporal multiplexing. Furthermore, it may be possible to design filter pairs to improve color discrimination for people with color vision deficiencies, for example creating up to four effective cone types in dichromats. This technology could be integrated in a simple pair of eyeglasses or sunglasses, and could have immediate applications in camouflage detection, quality control and anti-counterfeiting. More broadly, the ability to see many more colors has intriguing opportunities for design and artwork, and for data representation with extra color channels.

### **Acknowledgments:**

We thank Middleton Spectral Vision for access to their hyperspectral imaging systems. This work was supported by startup funds from UW Madison. B. Gundlach is supported by the National Science Foundation Graduate Research Fellowship under Grant No. DGE-1256259.

## **References:**

1. Schnapf JL, Kraft TW, Baylor DA (1987) Spectral sensitivity of human cone photoreceptors. *Nature* 325(6103):439–441.
2. Stockman A, Sharpe LT (2000) The spectral sensitivities of the middle- and long-wavelength-sensitive cones derived from measurements in observers of known genotype. *Vision Res* 40(13):1711–1737.
3. Mollon JD (1999) Color vision: Opsins and options. *Proc Natl Acad Sci* 96(9):4743–4745.
4. Backhaus W, Kliegl R, Werner JS (1998) *Color Vision: Perspectives from Different Disciplines* (Walter de Gruyter).
5. Colorimetry, 3rd ed. (2004) (CIE Central Bureau, Vienna).
6. Wyszecki G, Stiles WS (2000) *Color Science: Concepts and Methods, Quantitative Data and Formulae* (Wiley-Interscience, New York). 2nd edition.
7. Evolution of ultraviolet vision in the largest avian radiation - the passerines (2011) *BMC Evol Biol* 11(1):313–320.
8. Nathans J, et al. (1989) Molecular Genetics of Human Blue Cone Monochromacy. *Science* 245(4920):831–838.
9. Jordan G, Deeb SS, Bosten JM, Mollon JD (2010) The dimensionality of color vision in carriers of anomalous trichromacy. *J Vis* 10(8):12–12.
10. Tanaka G, Suetake N, Uchino E (2010) Lightness modification of color image for protanopia and deuteranopia. *Opt Rev* 17(1):14–23.
11. Neitz J, Neitz M, Jacobs GH (1993) More than three different cone pigments among people with normal color vision. *Vision Res* 33(1):117–122.
12. Neitz M, Neitz J, Grishok A (1995) Polymorphism in the number of genes encoding long-wavelength-sensitive cone pigments among males with normal color vision. *Vision Res* 35(17):2395–2407.
13. Neitz J, Jacobs GH (1990) Polymorphism in normal human color vision and its mechanism. *Vision Res* 30(4):621–636.
14. Nagy AL, MacLeod DIA, Heyneman NE, Eisner A (1981) Four cone pigments in women heterozygous for color deficiency. *JOSA* 71(6):719–722.
15. Jameson KA, Highnote SM, Wasserman LM (2001) Richer color experience in observers with multiple photopigment opsin genes. *Psychon Bull Rev* 8(2):244–261.
16. Jordan G, Mollon JD (1993) A study of women heterozygous for colour deficiencies. *Vision Res* 33(11):1495–1508.

17. Schmeder AW, McPherson DM (2014) Multi-band color vision filters and method by lp-optimization. Available at: <http://www.google.com/patents/US20140233105> [Accessed February 1, 2017].
18. Knoblauch K, McMahon MJ (1995) Discrimination of binocular color mixtures in dichromacy: evaluation of the Maxwell-Cornsweet conjecture. *J Opt Soc Am A Opt Image Sci Vis* 12(10):2219–2229.
19. Richer SP, Adams AJ, Little AC (1985) Toward the Design of an Optimal Filter for Enhancement of Dichromat Monocular Chromatic Discrimination. *J Optom* 62(2):105–110.
20. Zeltzer HI (1972) Method of improving color discrimination. Available at: <http://www.google.com/patents/US3701590> [Accessed February 1, 2017].
21. Pye DC, Dain SJ (1988) The X-Chrom lens: a case study. *Clin Exp Optom* 71(3):91–93.
22. Polzella DJ, Montgomery DA (1993) Dimensions of color harmony. *Bull Psychon Soc* 31(5):423–425.
23. Colorimetry -- Part 2: CIE standard illuminants (2007). ISO 11664-2
24. Robertson AR (1977) The CIE 1976 Color-Difference Formulae. *Color Res Appl* 2(1):7–11.
25. Colorimetry -- Part 6: CIEDE2000 Colour-difference formula (2014). ISO 11664-6
26. Colorimetry -- Part 4: CIE 1976 L\*a\*b\* Colour space (2008). ISO 11664-4
27. Wales DJ, Doye JPK (1997) Global Optimization by Basin-Hopping and the Lowest Energy Structures of Lennard-Jones Clusters Containing up to 110 Atoms. *J Phys Chem A* 101(28):5111–5116.
28. Powell MJD (1994) A Direct Search Optimization Method That Models the Objective and Constraint Functions by Linear Interpolation. *Advances in Optimization and Numerical Analysis, Mathematics and Its Applications.*, eds Gomez S, Hennart J-P (Springer Netherlands), pp 51–67.
29. Berns RS, Motta RJ, Gorzynski ME (1993) CRT colorimetry. part I: Theory and practice. *Color Res Appl* 18(5):299–314.
30. Sharma G (2002) LCDs versus CRTs-color-calibration and gamut considerations. *Proc IEEE* 90(4):605–622.
31. Vukusic P, Sambles JR, Lawrence CR, Wootton RJ (1999) Quantified interference and diffraction in single Morpho butterfly scales. *Proc R Soc Lond B Biol Sci* 266(1427):1403–1411.
32. Bulina ME, et al. (2004) New class of blue animal pigments based on Frizzled and Kringle protein domains. *J Biol Chem* 279(42):43367–43370.

## Supplementary Information

### Enhancing human color vision by breaking binocular redundancy

Bradley S. Gundlach<sup>1</sup>, Alireza Shahsafi<sup>1</sup>, Gregory Vershbow<sup>2</sup>, Chenghao Wan<sup>1,3</sup>, Jad Salman<sup>1</sup>,  
Bas Rokers<sup>4,5</sup>, Laurent Lessard<sup>1</sup>, Mikhail A. Kats<sup>1,3,5\*</sup>

<sup>1</sup>Department of Electrical and Computer Engineering, University of Wisconsin-Madison

<sup>2</sup>Department of Art, University of Wisconsin-Madison

<sup>3</sup>Department of Materials Science and Engineering, University of Wisconsin-Madison

<sup>4</sup>Department of Psychology, University of Wisconsin-Madison

<sup>5</sup>McPherson Eye Research Institute, University of Wisconsin-Madison

#### Conversion between a spectrum, XYZ tristimulus values, and LAB:

To calculate the perceived color of light through a visible-wavelength transmission filter, the following equation is used:

$$\Theta = \int_{\lambda_1}^{\lambda_2} \bar{\theta}(\lambda) T(\lambda) I(\lambda) d\lambda / \int_{\lambda_1}^{\lambda_2} \bar{y}(\lambda) I(\lambda) d\lambda$$

where  $\Theta = [X; Y; Z]$  are the XYZ tristimulus values,  $\bar{\theta}(\lambda) = [\bar{x}(\lambda), \bar{y}(\lambda), \bar{z}(\lambda)]$  are the CIE standard observer matching functions [1],  $T(\lambda)$  is the transmission spectrum of the filter, and  $I(\lambda)$  is the spectral power of the light passing through the filter. The XYZ tristimulus values can then be transformed to a different color space; in this work, we use the LAB color space because it allows for straightforward color difference calculations. The transformation describing the conversion from XYZ to LAB tristimulus values is given by [2]:

$$L_1 = 116f\left(\frac{Y}{Y_n}\right) - 16, a_1 = 500\left[f\left(\frac{X}{X_n}\right) - f\left(\frac{Y}{Y_n}\right)\right], b_1 = 200\left[f\left(\frac{Y}{Y_n}\right) - f\left(\frac{Z}{Z_n}\right)\right]$$

Where

$$f(t) = \begin{cases} t^{1/3}, & t > \left(\frac{6}{29}\right)^3 \\ \frac{1}{3}\left(\frac{6}{29}\right)^2 t + \frac{4}{29}, & \text{otherwise} \end{cases}$$

and  $X_n, Y_n, Z_n$  are the tristimulus values of the reference white point (95.047, 100.000, 108.883 for Illuminant D65) [3].

### *Narrative explanation of the filter design process*

The filters in this work were designed using a white-balance condition that ensures that broadband “white light” that passes through the two filters is perceived similarly, to prevent significant color clashing between the two eyes under typical viewing conditions. Simultaneously, the filters are designed to be sufficiently distinct, which results in each eye receiving different spectral information. We used a design approach where each revision increased in complexity, building intuition at each design stage.

For the first revision, a brick-wall longpass filter and a bandstop filter were used to split the blue cone response without significantly affecting the other cone types (Fig. S1). The filters were constrained such that the longpass filter cut-on wavelength was equal to the bandstop filter cut-off wavelength, which ensured that at least one eye was sensitive to every region of the visible wavelengths (*i.e.*, no wavelength was attenuated by both filters). The bandstop filter cut-on wavelength was chosen to be 450 nm to minimize the effect of the filters on the M and L cone responses; thus, we were left to decide the longpass cut-on and bandstop cut-off wavelengths (which are enforced to be equal), and which must be below 450nm. With these constraints, the position of the cut-on/cut-off wavelength was optimized in order to minimize the CIE  $\Delta E$  color difference between D65 white light passing through each filter. Figure S1(a) shows the result of this optimization, with a minimum  $\Delta E$  color difference of 0.596 with the cut-on/cut-off wavelength at 437 nm. A  $\Delta E$  color difference less than 2.3 typically means that the colors are indistinguishable. The resulting optimized filters are: a longpass filter (filter 1) with a 437 nm transition wavelength, and a bandstop filter (filter 2) with a stopband of 437 - 450 nm. Figure S1(c) shows the rendered color of D65 white light through each filter, and demonstrates the excellent white-balance between filters, because the color samples are indistinguishable. However, the bandstop width of the resulting filter 2 is only 13 nm, quite low in comparison to the ~300 nm range of the visible wavelengths. In order to effectively differentiate spectral features, which are typically quite broad (>10 - 20 nm), the bandstop width must be larger.

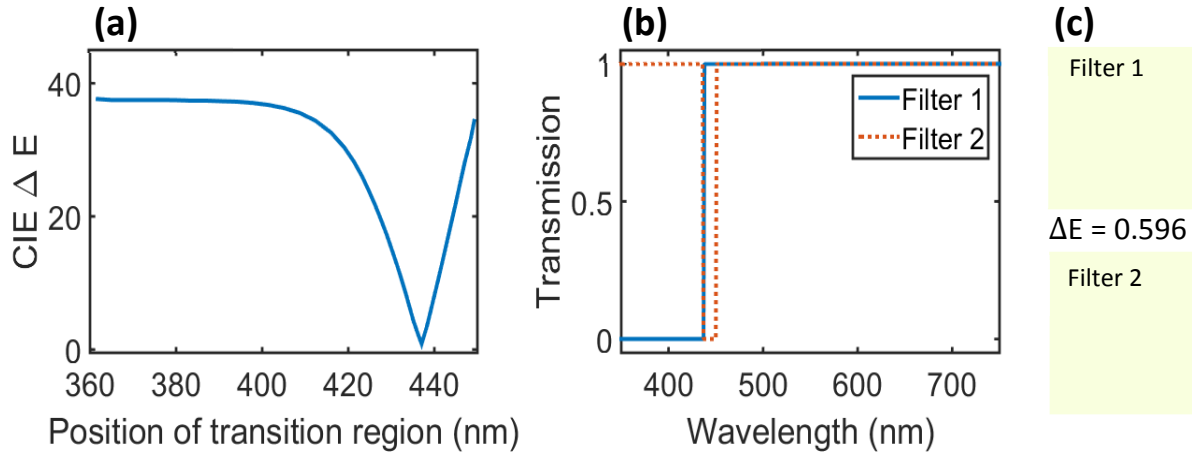


**Figure S1:** (a) Plot showing the CIE  $\Delta E$  color difference between filters 1 and 2 when transmitting CIE D65 white light versus cut-on/cut-off wavelength. (b) Optimized transmission response for filters 1 and 2 after the first design revision, with a band-stop region between 437 – 450 nm. (c) Rendered colors for CIE D65 white light transmitted through each filter from (b), with an optimized  $\Delta E$  color difference of 0.596.

Because this initial design produced a filter set with good white-balance, the same general approach was used in the following design revision. A similar optimization was performed as above, but the bandstop width of filter 2 was constrained to be larger than 25 nm; this width was chosen such that it was larger than many typical spectral features found in nature, which could therefore be resolved with these filters. Instead of minimizing just the  $\Delta E$  color difference between the filters, a modified merit function (MF) was used that also accounted for the filter width:  $MF = \Delta E / Width_{bandstop}$ . A brute-force optimization was performed, which varied the cut-on and cut-off wavelengths of the two filters (again with the longpass cut-on and bandstop cut-off wavelengths being equal). The transmission spectra of the optimized filters are given in Figure S2: a longpass filter (filter 1) with a 450 nm cut-on wavelength, and a bandstop filter (filter 2) with a stopband of 450 – 500 nm. The resulting filter set has a  $\Delta E$  color difference of 14.15, significantly above the 2.3 just noticeable difference threshold. Therefore, it is clear that for the simple design using a longpass and single-bandstop filter, there is a tradeoff between white-balance and width of the band stop region.

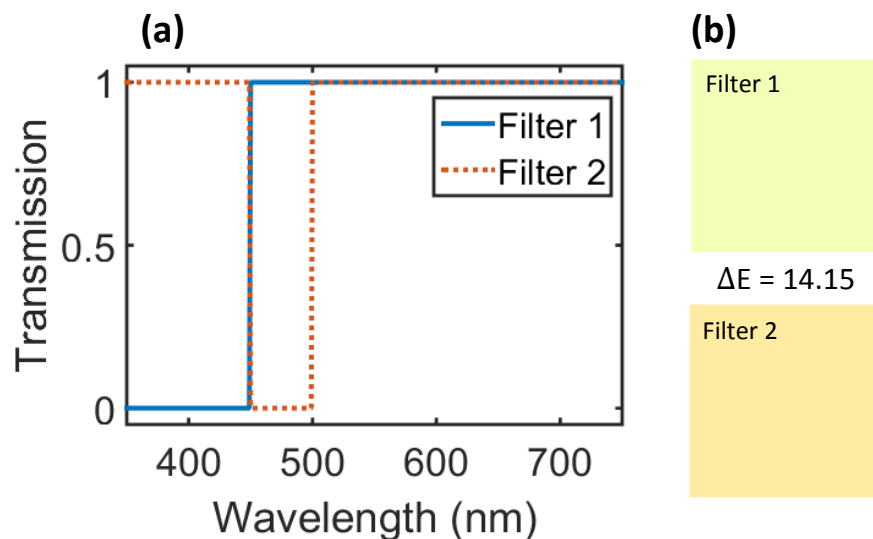


**Figure S2:** (a) Optimized transmission response for filters 1 and 2 after the second design revision, with a band-stop region of 450 - 500 nm. (b) Rendered colors for CIE D65 white light transmitted through each filter from (b), with an optimized  $\Delta E$  color difference of 14.15

By considering the cone responses (Figure 1(a)), it is clear why this filter design results in worse white balance. Beyond 450 nm, the longpass filter allows all wavelengths of visible light through; the M and L cones have very little response below 450 nm. However, the bandstop filter attenuates wavelengths between 450 and 500 nm, where the M and L cones have significant sensitivity. Therefore, the two filters affect the M and L cones very differently, which results in poor color balance. In particular, the bandstop filter (filter 2) introduces a slight red tint compared to the longpass filter (filter 1), which is also clear from the rendered colors in figure S2. Therefore, in order to maintain the high band-stop width of filter 2 while improving the white balance of the filter pair, a second stopband was introduced to filter 2 in order to soften the “red response” of the previous design. In this design, the shorter wavelength band-stop region of filter 2 splits the S cone, whereas the longer wavelength band-stop region improves the white balance of the filter pair.

In the final design revision that was implemented and described in the main text, the response of the longpass filter (filter 1) was not optimized any further; in fact, the transmission response of a commercially available 450 nm longpass filter was used to define filter 1. This was done to decrease manufacturing costs, such that only filter 2 required custom design and manufacturing. The short-wavelength bandstop region of the filter 2 was also used from before (allowed to change only slightly during optimization), and a preliminary long wavelength bandstop region was added between 600 and 700 nm, to be optimized further. An error function was also implemented to smooth the transition regions; in the



previous design revisions, the transition regions had a sharp vertical slope, which is difficult to achieve in practice. The smoothness of the filters can be adjusted by changing the proportionality constant ( $a$ ) of the error function:  $y = \text{erf}(ax)$ .

Unlike the previous revisions, filter 2 was optimized using a more rigorous method compared to the brute force method used above. A constrained optimization by linear approximation (COBYLA) method was implemented in a stochastic basin-hopping algorithm to optimize the position of the cut-on/cut-off wavelengths, transmission of the pass and stop-bands, and slope of the transition regions. The transition regions of the filter's short-wavelength band-stop region was constrained within  $\pm 10$  nm of their previous values; this was done to maintain the overall shape of the previous design while allowing some room for color balance optimization. The transmittance was constrained between 5 and 15% in the stopbands, and between 80 and 95% in the passbands, to allow for high throughput and relative ease of manufacturing. The error function proportionality constant was constrained between 0.25 and 1. The long-wavelength stopband region was constrained between 600 – 700 nm, but the bandstop width was not constrained; this was done to prevent attenuation of the M and L cones at their peak sensitivities ( $\sim 550$ nm,  $\sim 580$  nm respectively), while also preventing needless optimization beyond the visible wavelengths ( $> 700$  nm). With these constraints in place, filter 2 was optimized in order to minimize the modified merit function:  $\Delta E / \text{Width}_{\text{bandstop}}$ , where  $\Delta E$  is the color difference between filter 1 and filter 2 when transmitting D65 white light and  $\text{Width}_{\text{bandstop}}$  is the spectral width of the short-wavelength band-stop region of filter 2. This procedure yielded an optimized response for filter 2 with stopbands at 450 - 500 nm and 630 - 680 nm, and stopband/passband transmittance of 10% and 90%, respectively (Figure S3(a)). The rendered color of transmitted D65 white light through the filters is given in Figure S3(b), with a  $\Delta E$  color difference of 5.21.

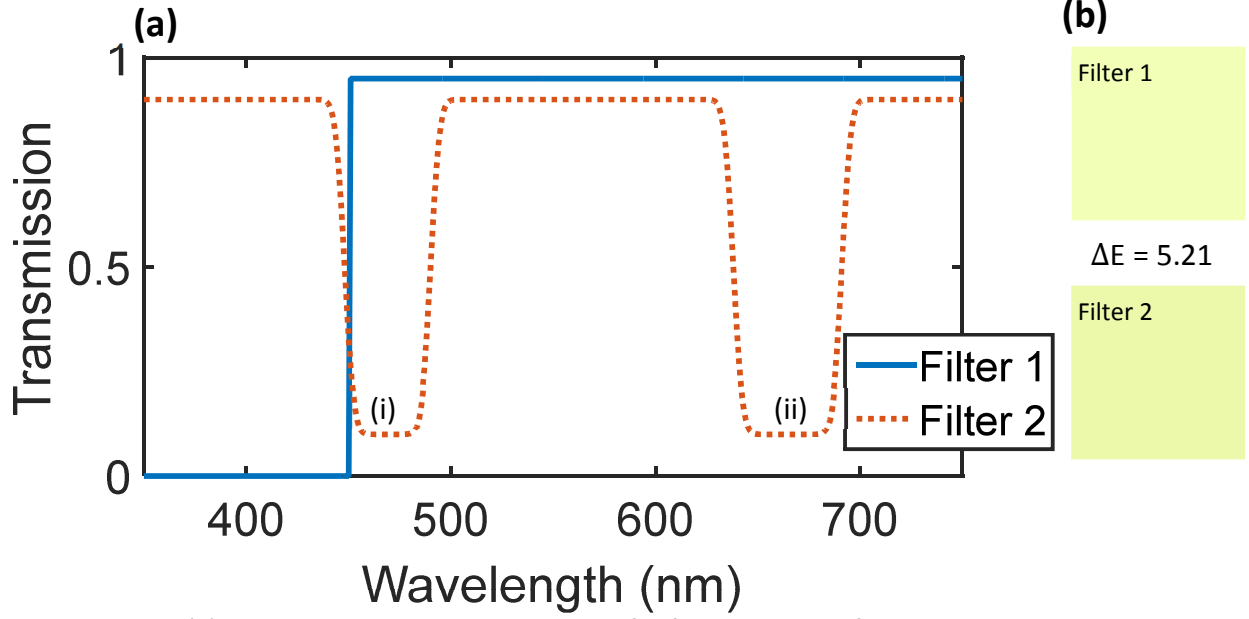


**Figure S3:** (a) Optimized transmission response for filters 1 and 2 after the third design revision, with band-stop regions between 450 – 500 nm (i) and 630 – 680 nm (ii). Region (i) splits the short-wavelength cone, region (ii) improves the white-balance of the filter pair (b) Rendered colors for CIE D65 white light transmitted through each filter from (a), with a  $\Delta E$  color difference of 5.21.

#### Methodology for counting metamers:

In this section, we describe the technique by which we estimated the reduction of the occurrence of metamerism using our vision enhancement device.

Each spectrum  $I(\lambda)$  is mapped to LAB tristimulus values  $[L, a, b]$  via the CIE matching functions described earlier in the supplementary. Counting the number of metamers for a particular LAB reference point  $[L_0, a_0, b_0]$  amounts to counting the number of different spectra  $I(\lambda)$  that map to tristimulus values that are within a sphere in LAB space of radius  $\Delta E$  of the reference point. The number of metameric spectra is infinite, so we instead compute a surrogate quantity. Roughly, we discretize each spectrum by wavelength so each spectrum can be abstracted as a point in a finite-dimensional space. We then count metamers by computing the volume that they occupy in this space. The details of the computation are described below.

1. Represent spectra by using  $M$  equally spaced samples in wavelength. For example,  $I(\lambda)$  is represented as a vector  $[I_1, I_2, \dots, I_M]$ , which corresponds to the intensities at the wavelengths  $[\lambda_1, \lambda_2, \dots, \lambda_M]$ .

2. The map  $[I_1, \dots, I_M] \rightarrow [L, a, b]$  from the discretized spectrum to LAB tristimulus values is smooth and nonlinear. Since the map is only being evaluated in a local neighborhood of the reference point, the map is well approximated by its first order Taylor expansion. This allows us to replace the nonlinear map with an affine function  $g(I_1, \dots, I_M) = [L, a, b]$ .
3. Let  $S_0 = \{ [L, a, b] \mid (L - L_0)^2 + (a - a_0)^2 + (b - b_0)^2 \leq \Delta E^2 \}$  be the set of tristimulus values indistinguishable from the reference point. The set of metameric spectra is given by the image of  $S_0$  under the inverse map  $g^{-1}$ .
4. Since the inverse map  $g^{-1}$  is affine and the set  $S_0$  is a sphere in LAB space, the image  $g^{-1}(S_0)$  is an ellipsoid in the discretized spectrum space [4]. Note that this ellipsoid is degenerate; it will be infinite in the directions corresponding to the kernel of  $g$ .
5. We assume that we are counting “reflection metamers” or “transmission metamers” under a certain illuminant. That is, we are excluding metamers generated by active emissive sources for the sake of this calculation, since including unbounded emissive sources complicates this calculation further. Under this assumption, the allowed intensities are not infinite, since every admissible spectrum has intensities bounded by the corresponding intensities of the illuminant. More formally, define the set of admissible spectra as  $C_0 = \{ [I_1, \dots, I_M] \mid 0 \leq I_k \leq I_k^{D65} \text{ for } k = 1, \dots, M \}$ , where  $I_k^{D65}$  is the intensity at  $\lambda_k$  of the D65 illuminant.
6. The volume of metameric spectra is therefore the volume of the set  $g^{-1}(S_0) \cap C_0$ .

If the spectrum is filtered through a filter  $T(\lambda)$ , the map  $g$  must be replaced by a map  $g_T$  that accounts for the filter  $T$ . The derivation is otherwise identical; metameric spectra are given by the set  $g_T^{-1}(S_0) \cap C_0$ . If the spectrum is filtered through  $T_1(\lambda)$  for one eye and  $T_2(\lambda)$  for the other eye, spectra are only counted if they are metameric for *both* eyes. This results in the set  $g_{T_1}^{-1}(S_0) \cap g_{T_2}^{-1}(S_0) \cap C_0$ .

We can compare configurations (e.g. natural human vision versus vision augmented by our device, or vision augmented by two different filters sets) by comparing the volumes of their respective metameric spectra. For example, to compare the unfiltered case (natural human vision) to the case of vision modified by our two-filter passive multispectral device, we would compute the ratio:

$$\rho = \frac{\text{Vol}(g^{-1}(S_0) \cap C_0)}{\text{Vol}(g_{T_1}^{-1}(S_0) \cap g_{T_2}^{-1}(S_0) \cap C_0)}$$

A ratio of  $\rho = 20$  would signify that metameric spectra are 20 times less abundant when the two-filter passive multispectral device is used as compared to the unfiltered case. Specifically, if spectra are sampled from a uniform distribution on intensities, a spectrum is 20 times less likely to be metameric.

Computing the ratio  $\rho$  is challenging because the volumes involved have irregular shapes; they are intersections of degenerate (high-dimensional) ellipsoids with box constraints. In order to approximate the ratio  $\rho$ , we approximate each volume by the volume of its max-volume inscribed ellipsoid. An illustration of a max-volume inscribed ellipsoid is shown below (Fig. S4).

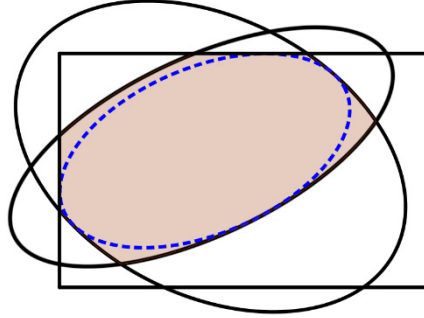


**Figure S4** – The shaded region is the intersection of ellipsoids and box constraints. The area is approximated by the max-area inscribed ellipsoid (dotted curve).

It turns out the max-volume inscribed ellipsoid can be efficiently computed using semidefinite programming techniques. See for example [5]. We approximated the ratio  $\rho$  by using the inner ellipsoid approximation for both the numerator and denominator. Volume approximation ratios were computed using CVX, a package for specifying and solving convex programs [6]. We computed approximate volume ratios for the two-filter case as well as the one-filter case, using the transmission spectrum of a filter sold by EnChroma for alleviating some of the adverse effects of red-green color vision deficiency (EnChroma filter [7]). In each case, we tried several different discretization samples  $M$  and we repeated the computation for 500 different reference points  $[L_0, a_0, b_0]$ . The reference points were selected by choosing discretized spectra uniformly at random and mapping them to LAB tristimulus values. A summary of the results is shown in Table S1. Using two filters results in a dramatic decrease in metamers, roughly consistent over the range of tested discretizations. In contrast, using a single filter (EnChroma in this case) has little effect on the number of metamers.

Discretization samples ( $M$ )	7	9	12	14	16	18
Two filters, mean	22.977	115.823	120.580	160.634	178.020	111.243
Two filters, median	17.251	80.690	57.4080	85.885	77.153	41.369
EnChroma, mean	0.945	0.887	1.090	0.944	1.125	1.086
EnChroma, median	0.945	0.870	1.082	0.944	0.924	1.017

**Table S1** – Results of the metamer ratio approximation. Mean and median  $\rho$  values are computed over 500 randomly generated spectra for each discretization. Using two filters reduces the frequency of metamers by a factor of about 50 on average, while using a single EnChroma filter has a negligible effect on the frequency of metamers

### Thin-film filter design

The filter response design goal (Fig. S3(a)) used in this work is realized by conventional thin-film design methods. A commercial thin-film design software (Optilayer) was used to optimize a two-material thin-film stack to adequately meet the design goal. Tantalum oxide ( $\text{Ta}_2\text{O}_5$ ) was chosen as the high index ( $n = 2.15$ ) material and silicon dioxide ( $\text{SiO}_2$ ) was chosen as the low index ( $n = 1.46$ ) material, as they are both easily deposited. The substrate was NBK7, a common optical glass. The final stack was constrained to be less than 75 total layers to keep costs down, and each layer between 10 – 500 nm to prevent stress cracks in thick films. Using these constraints in tandem with the provided filter design goal, the thin-film stack was optimized for incident angles between 0 - 10°. A representative stack design produced by Optilayer for the design of filter 2 is given below (Fig. S5):

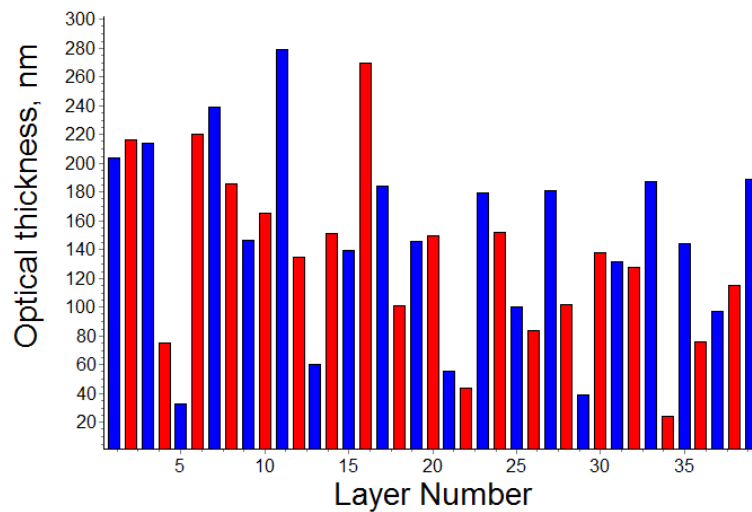


**Figure S5:** Thin-film filter stack design for filter 2 (Fig. S3(a)), using  $\text{Ta}_2\text{O}_5$  ( $n = 2.15$ , blue) and  $\text{SiO}_2$  ( $n = 1.46$ , red) dielectric layers.

The actual design for the device experimentally demonstrated in the main text was slightly modified from that of Fig. S5 by a thin-film foundry (Iridian), and the final design cannot be shared due to a non-disclosure agreement. Nevertheless, the specifics of the design are not critical as long as it implements the desired transmission spectrum (Fig. 2(b)).

### **Comparison of CRT and LCD monitors:**

The displays used in this work to generate metameric spectra were a True HD-IPS liquid crystal display (LCD) on a LG G3 smartphone and a conventional cathode ray tube (CRT) monitor (Dell E770P). These displays use very different mechanisms to generate colors, which results in significantly different spectra when displaying the same color (i.e. metamers). The LCD display uses a backlight, typically a white LED, which is transmitted through color filter arrays (red, green and blue color filters) to produce its color response. Therefore, the emitted spectrum is the product of the LCD backlight and color filter transmission response. The CRT monitor uses an electron gun, and relies on a phosphorescent screen to control its spectrum in the visible wavelength range. Because the two display types use significantly different methods to generate colors, the two emission technologies have different spectral features for the individual red, green and blue color channels. The distinct features of the two displays are demonstrated in Figure S6(a), which shows the measured emitted spectrum of white light from each display (RGB = [255, 255, 255]). Figures S6(b, c) show the spectrum of each pure color channel (red, green and blue) for the LCD and CRT display, respectively.

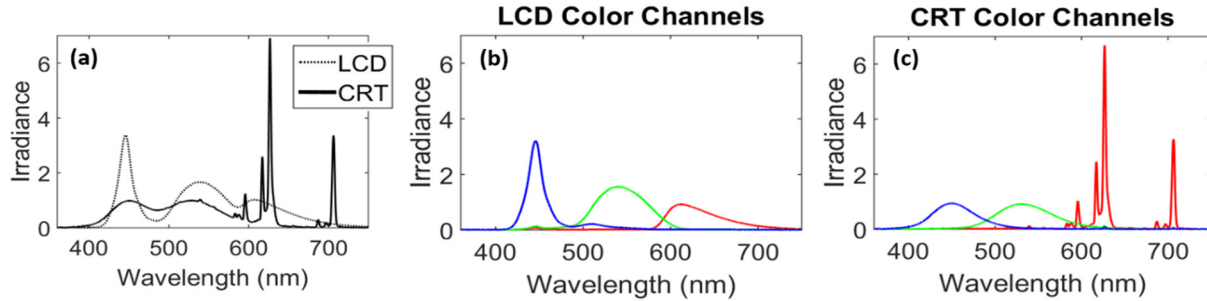


**Figure S6:** (a) Measured emission spectra of the LCD and CRT displays used in this work, displaying a white color (RGB = 255, 255, 255). (b, c) Measured emission spectra of each individual color channel (R, G, B) for the LCD and CRT display, respectively. For blue curves, the displayed color was RGB = (0, 0, 255), red curves RGB = (255, 0, 0), and green curves RGB = (0, 255, 0)

### **Color accuracy of photographs:**

In this work, we used digitally generated color samples from spectroscopic data to demonstrate the splitting of a metameric pair using an LCD and CRT monitor (Fig. 3). This method was used because, due to the difference in spectral response between a camera sensor and the human eye, it is difficult to obtain a precisely color-accurate photograph. This difficulty is shown in Figure S7, which shows the original photograph of the experimental setup in Fig. 3(c), an edited photograph that better approximates the actual color, and a digitally rendered color sample showing the “actual color”. The colors are rendered using CIE matching functions, as described above; the  $[X,Y,Z]$  values calculated using the matching functions and the measured spectrum can then be converted to the sRGB color space, which is the working color space of most computers. Though the sRGB values will be the same across all display devices, the actual displayed color depends on the calibration of the monitor used. Therefore, the rendered color in Fig. S7(c) only represents the perceived color seen in the experiment when the monitor used to view the image has a perfect color calibration.

It is clear that Fig. S7(a) is significantly different than the generated color sample in Fig. S7(c), even though the camera used in S7(a) and the spectrometer used to acquire the sample that generated the color in S8(c) sampled the same light. Fig. S7(b) is the figure used in the main text (Fig. 3(b)), and was edited to more closely represent the color in S8(c) to prevent confusion. The rendered color samples using spectroscopic data represent the perceived colors of both monitors much more accurately.

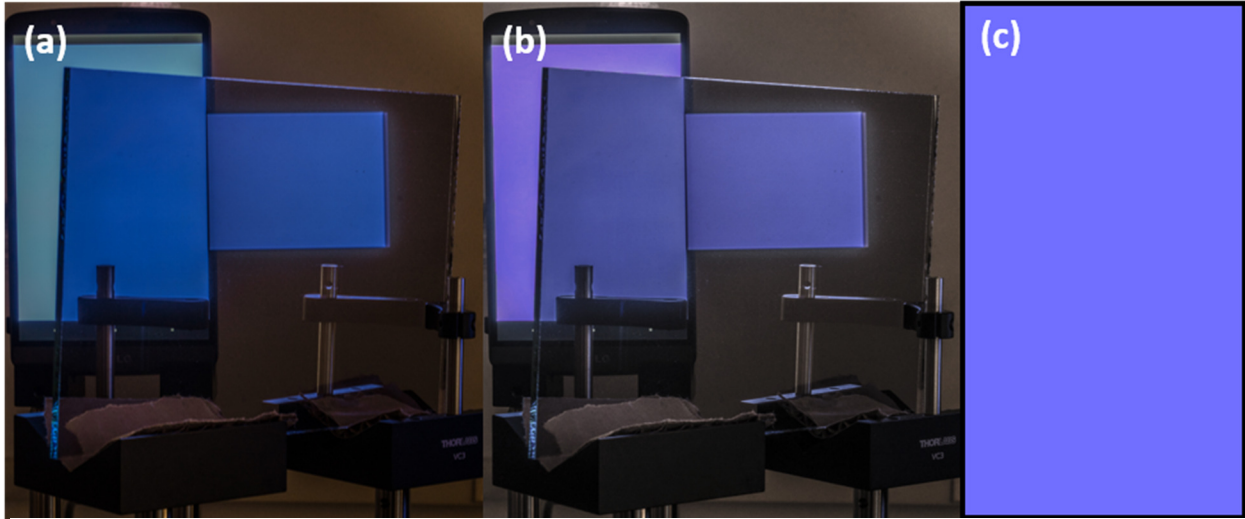


**Figure S7:** (a) Photograph of the setup shown in Fig. 3(c) of the main text, taken using a Sony  $\alpha 7R II$  camera. (b) The edited photograph that appears in Fig. 3(b) of the main text, which was modified to appear close in color to the rendered colors. This manipulation was performed to prevent confusion in the main text. (c) The actual color displayed during the experiment, rendered using spectra acquired using a grating spectrometer and cosine corrector.

### **Supplementary References**

- S1. Colorimetry -- Part 1: CIE standard colorimetric Observers (2007). ISO 11664-1
- S2. Wyszecki G, Stiles WS (2000) *Color Science: Concepts and Methods, Quantitative Data and Formulae* (Wiley-Interscience, New York). 2nd edition.
- S3. Colorimetry -- Part 2: CIE standard illuminants (2007). ISO 11664-2
- S4. Giuseppe C, Ghaoui LE (2014) *Optimization Models* (Cambridge University Press).
- S5. Boyd S, Vandenberghe L (2004) *Convex optimization* (Cambridge University Press).
- S6. Grant M, Boyd S *CVX: Matlab software for disciplined convex programming*, version 2.1, <http://cvxr.com/cvx>, October 2016.
- S7. Schmeder AW, McPherson DM (2014) Multi-band color vision filters and method by lp-optimization. Available at: <http://www.google.com/patents/US20140233105> [Accessed February 1, 2017].